Journal of Controlled Release 380 (2025) 818–828

Contents lists available at ScienceDirect

Journal of Controlled Release

journal homepage: www.elsevier.com/locate/jconrel

Multidrug micelles and sonopermeation for chemotherapy co-delivery to brain tumors

Anshuman Dasgupta [a], Jan-Niklas May [a], Geir Klinkenberg [b], Helena C. Besse [c], Eva Miriam Buhl [d], Diana Moeckel [a], Rahaf Mihyar [a], Quim Peña [a], Armin Azadkhah Shalmani [a], Christopher Hark [a], Anne Rix [a], Susanne Koletnik [a], Josbert Metselaar [a], Yang Shi [a], Wim E. Hennink [e], Gert Storm [e,f], Dannis van Vuurden [g], Chrit Moonen [h], Mario Ries [c], Ruth Schmid [b], Fabian Kiessling [a], Twan Lammers [a,*]

[a] Institute for Experimental Molecular Imaging, Uniklinik RWTH Aachen, Aachen, Germany
[b] Department of Biotechnology and Nanomedicine, SINTEF Industry, Trondheim, Norway
[c] Center for Imaging Sciences, University Medical Center Utrecht, Utrecht, the Netherlands
[d] Electron Microscopy Facility, Institute of Pathology, Uniklinik RWTH Aachen, Aachen, Germany
[e] Department of Pharmaceutics, Utrecht University, 3584 CG Utrecht, the Netherlands
[f] Department of Surgery, National University of Singapore, 119228 Singapore, Singapore
[g] Princess Maxima Center for Pediatric Oncology, Utrecht, the Netherlands
[h] Imaging and Oncology Division, University Medical Center Utrecht, Utrecht, the Netherlands

ARTICLE INFO

Keywords:
Nanomedicine
Tumor targeting
Combination therapy
Brain cancer
DIPG

ABSTRACT

Brain tumors are difficult to target and treat. The blood-brain barrier (BBB) limits drug delivery to pathological sites, and standard mono-chemotherapy typically results in suboptimal efficacy and development of drug resistance. We here set out to load a synergistic drug combination in polymeric micelles, and combined them with ultrasound- and microbubble-mediated BBB opening in glioma models in mice. Via high-throughput screening of various chemotherapy combinations in different glioma cell lines, valrubicin and panobinostat were identified as a synergic drug combination and *co*-loaded in mPEG-*b*-p(HPMAm-Bz)-based polymeric micelles. Intravenous administration of double-drug micelles showed good tolerability and resulted in significant tumor growth inhibition in mice with subcutaneous GL261 gliomas. In orthotopically inoculated patient-derived HSJD-DIPG-007 diffuse intrinsic pontine gliomas, notoriously known to have an intact BBB and poor drug responsiveness, we provide initial experimental evidence showing that multidrug micelles plus sonopermeation can help to improve treatment efficacy. Our work exemplifies that synergistic drug combinations can be efficiently *co*-loaded in polymeric micelles, and that advanced nanosonochemotherapy combination regimens hold promise for the treatment of hard-to-treat brain tumors.

1. Introduction

Brain tumors, especially glioblastoma multiforme (GBM) and diffuse intrinsic pontine glioma (DIPG), are difficult to treat and have a very poor prognosis [1,2]. Surgery is often inoperable, especially in case of tumors located in or infiltrating the brain stem [1,2]. Administering mono-chemotherapy has been the standard of care, but has several downsides. Firstly, single drug therapies rapidly result in drug resistance and do not produce significant therapeutic efficacy [3]. Secondly, most standard chemotherapeutic drugs have – in general – suboptimal pharmacokinetics, resulting in low target-site accumulation and high off-target localization, thereby resulting in a poor balance between efficacy and toxicity [4]. Moreover, the blood-brain barrier (BBB), which is characterized by inter-endothelial cell tight junctions, severely limits the delivery of chemotherapy drugs to brain tumors [5,6].

Several strategies have been explored to improve drug delivery to and anti-tumor efficacy against brain tumors. With regard to small molecules, multidrug combinations offer key advantages over mono-drug therapy. Drug combinations with different mechanisms of action can target multiple pathways in cancer cells [3,7]. This type of treatment

* Corresponding author.
E-mail address: tlammers@ukaachen.de (T. Lammers).

https://doi.org/10.1016/j.jconrel.2025.02.018
Received 29 November 2024; Received in revised form 28 January 2025; Accepted 8 February 2025
Available online 19 February 2025

regimen reduces the likelihood of developing drug resistance and typically enable inductions of synergistic anti-tumor effects [3,7]. For example, pairing the AXL tyrosine kinase inhibitor bemcentinib with the histone deacetylase inhibitor (HDACi) panobinostat demonstrated synergy across a range of DIPG models [8], illustrating that optimal drug combinations hold promise to promote therapeutic outcomes in difficult-to-treat brain tumors.

To optimize the pharmacokinetics of drug molecules and the efficacy of drug combinations, various nanomedicines have been employed, including liposomes and micelles. Nanomedicines are 1–100(0) nm-sized pharmaceutical formulations that aim to improve target site accumulation while minimizing off-target localization [9,10]. A prototypic example of a nanomedicinal drug product used for multi-drug delivery is Vyxeos®. This liposome formulation co-encapsulates daunorubicin and cytarabine at a fixed 1 to 5 M ratio, and it has shown significantly improved efficacy as compared to standard dual drug treatment in patients with secondary acute myeloid leukemia [11].

In patients with brain tumors wherein the BBB is intact, physical or pharmacological priming strategies are needed to help drugs and drug delivery systems reach the pathological site [4,5,10]. The combination of ultrasound (US) and microbubbles (MB), commonly referred to as sonoporation or sonopermeation, has been widely explored for this purpose [12]. MB are 1–10 μm-sized air-filled vesicles that are routinely used in the clinic as US contrast agents. In the presence of US, MB oscillation generates shear forces near vessel walls and endothelial cell membranes, promoting BBB permeability and nanomedicine delivery (in)to the brain [13,14]. Several ongoing efforts have demonstrated the clinical feasibility, efficacy and safety of sonopermeation as a means to open up the BBB in patients suffering from GBM [15,16].

Taking the above insights and advances into account, we set out to combine drug synergy, nanomedicine co-delivery and sonopermeation to improve the treatment of brain tumors. Anthracyclines, taxanes and HDACi were chosen as drug classes, as they have shown reasonably good efficacy against multiple brain tumor models [17–19]. In this study, four glioma cell lines were treated with combinations of anthracyclines, taxanes and HDACi, as pairing drugs with different mechanism of action can target multiple pathways in cancer cells, thereby inducing synergistic effects (Fig. 1A) [3,7]. The identified synergistic drug combination was *co*-encapsulated in polymeric micelles based on methoxy poly (ethylene glycol)-*b*-(*N*-(2-benzoyloxypropyl) methacrylamide) (i.e., mPEG-*b*-p(HPMAm-Bz)) block copolymers (Fig. 1B). The micelles were characterized in terms of physicochemical properties and drug loading and retention capabilities (Fig. 1B). Upon intravenous (i.v.) administration, the efficacy of the multidrug micelles was evaluated in a non-diffuse subcutaneous GL-261 glioma model, as well as – in combination with sonopermeation - in a diffuse HSJD-DIPG-007 model (Fig. 1C). Our findings showcase the effect of multidrug micelles and sonopermeation for improving the treatment of high-grade brain tumors.

2. Results

2.1. Anthracyclines and histone deacetylase inhibitors show synergistic drug activity against glioma cells

We incubated four glioma cell lines with different drug combinations to assess synergistic drug activity effects. The cell lines used were U-87 MG, GL-261, KNS-42, SF-8628. The drugs used were HDACi (panobinostat, vorinostat), taxanes (cabazitaxel, docetaxel, paclitaxel), and anthracyclines (epirubicin, pirarubicin, idarubicin, daunorubicin, valrubicin, doxorubicin), and they were tested at concentrations of 1, 10, 100 and 1000 ng/mL. Drugs from the three different classes were combined between them in all four cell lines (Fig. 2A). Finally, viability was assessed and synergy bliss excess was calculated based on the viability data (Supplementary Tables S1-S8).

Interestingly, the heat maps in Fig. 2D-E demonstrate that the combination of anthracyclines and taxanes induced strong antagonistic effects, especially in KNS-42 and SF-8628 cell lines. Analogously, the combination of taxanes and HDACi showed strong antagonistic effects (Fig. 2E). Based on these findings, combinations of anthracycline-taxane and taxane-HDACi were excluded for further evaluation. On the contrary, almost all anthracycline-HDACi combinations showed good synergistic effects in U-87MG and KNS-42 cell lines (Fig. 2B and D). Also, in GL-261 and SF-8628, distinct combinations of anthracycline and HDACi demonstrated synergism (Fig. 2C and E). These results exemplify that the combination of anthracycline and HDAC inhibitors holds promise for *co*-encapsulation into polymeric micelles for producing synergistic drug activity in glioma tumors.

2.2. Producing polymeric micelles co-loaded with anthracyclines and histone deacetylase inhibitors

We next sought to develop nanomedicine formulations which are able to efficiently co-encapsulate anthracyclines and HDACi. For this purpose, mPEG-*b*-p(HPMAm-Bz)-based micelles were employed, given their previously shown ability to (co-)encapsulate hydrophobic drugs in the core [20–22]. Among the available anthracyclines and HDACi, we chose valrubicin (VAL) and panobinostat (PAN), since: (1) they are characterized by high hydrophobicity, and log *P* values of 2.67 and 3.16, enabling efficient (co-) loading and retention in micelles [22]; (2) both drugs are FDA-approved; (3) PAN has previously demonstrated excellent anti-tumor efficacy in multiple brain tumor models including DIPG [17,19].

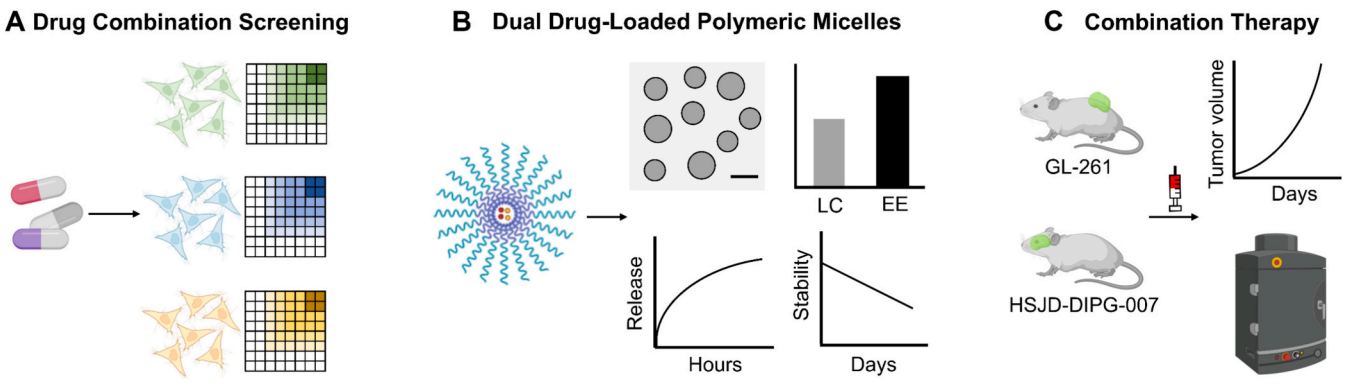

Fig. 1. Study setup. (A) Drug combinations were screened for synergy in multiple glioma cell lines. (B) Synergistic drug combinations were subsequently *co*-encapsulated in mPEG-*b*-p(HPMAm-Bz) polymeric micelles. The micelle formulation was characterized in terms of morphology, size, encapsulation efficiency, drug release, and shelf-life stability. (C) The multidrug-loaded micelles were i.v. administered and their therapeutic efficacy was assessed in the non-diffuse subcutaneous GL-261 glioma model and, in combination with MB- and US-mediated sonopermeation, in the orthotopic HSJD-DIPG-007 pons glioma model.

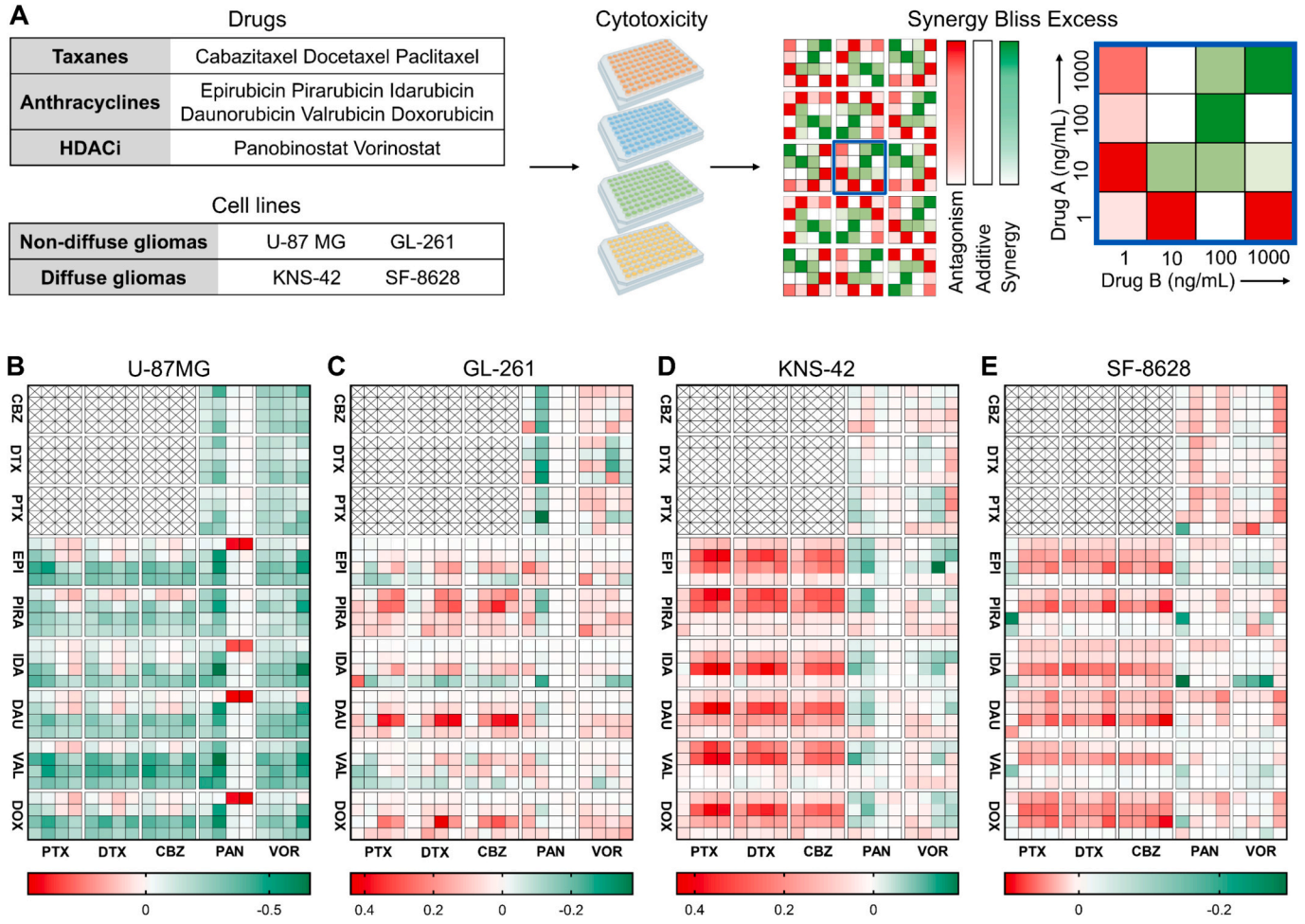

Fig. 2. Drug synergy screening in glioma cell lines. (A) Overview of the drug synergy screening experimental setup. Eleven drugs: cabazitaxel (CBZ), docetaxel (DTX), paclitaxel (PTX), epirubicin (EPI), pirarubicin (PIRA), idarubicin (IDA), daunorubicin (DAU), valrubicin (VAL), doxorubicin (DOX), panobinostat (PAN), vorinostat (VOR); and four glioma cell lines: U-87 MG, GL-261, KNS-42, SF-8628 were employed. Upon incubating glioma cells with drug combinations in vitro, synergistic efficacy was assessed. Antagonism, additive and synergy scores are colour-coded in red, white and green, respectively. (B-E) Representative heat maps, showing that certain specific combinations of anthracyclines and HDACi resulted in moderate to strong synergy across the glioma cell lines. Scores were evaluated using bliss excess method derived from viability data, and represented as mean of three independent experiments. (For interpretation of the references to colour in this figure legend, the reader is referred to the web version of this article.)

To achieve efficient co-encapsulation of VAL and PAN, the mPEG-*b*-p(HPMAm-Bz) polymer concentration was systematically increased during the micelle preparation (Fig. 3A). At increasing polymer concentration, the encapsulation efficiency (EE) of PAN was found to increase linearly, and for VAL the EE remained unchanged (Fig. 3B). Based on this, we used 80 mg/mL polymer and 3 mg/mL feed concentration of each drug to prepare the micelle formulation for our future experiments. This is because both VAL and PAN showed the highest EE and were co-loaded at a weight ratio of 1:1, enabling them to be administered at their respective maximum tolerated dose (indicated by red arrow; Fig. 3B-C). The optimized micelle formulation was subsequently characterized in terms of morphology, size, drug encapsulation, drug release and stability. TEM image confirmed that the VAL-PAN micelles exhibited homogeneous spherical morphology and a narrow size distribution (Fig. 3D). The double drug-loaded VAL PAN micelles displayed a mean size of 65 nm and polydispersity index <0.2 (Fig. 3E). Furthermore, both VAL and PAN were efficiently co-loaded in the micelles with an EE > 80 % and loading capacity >3 % (Fig. 3F).

To simulate drug release under physiologically relevant (sink) conditions, the micelles were placed in a dialysis bag immersed in 4.5 % w/v bovine serum albumin-containing PBS media at pH 7.4 and at 37 °C. We found that 50 % of PAN was activated from the micelles within 1 h, indicating rapid burst release (Fig. 3G). On the contrary, 50 % of VAL was released after 48 h, highlighting a more sustained release profile (Fig. 3G). The stability of the co-loaded micelle formulation was also evaluated by storing them for prolonged periods of time at room temperature. We found that the concentration, size and PDI of micelles did not show any significant change after 4 weeks of storage ($p > 0.05$; Fig. 3H-I). Furthermore, > 80 % of VAL and PAN were still retained inside the micelles after 4 weeks of storage (Fig. 3J). Together, these results indicate that using high polymer concentrations during the formulation preparation result in efficient co-encapsulation of VAL and PAN, homogeneous micelle size, and shelf-stable micelles at room temperature.

2.3. *Double-drug polymeric micelles improve anti-tumor efficacy in a subcutaneous mouse glioma model*

We evaluated the efficacy of VAL plus PAN co-loaded micelles (VAL PAN-PM) in two different brain tumor models. GL-261 was chosen as a subcutaneous glioma model, because it is well-characterized and partially amenable to nanoparticle therapy [23]. Upon subcutaneous inoculation of GL-261 glioma cells, mice were i.v. administered twice weekly at a dose of 6 mg/kg VAL and PAN either co-loaded in micelles or

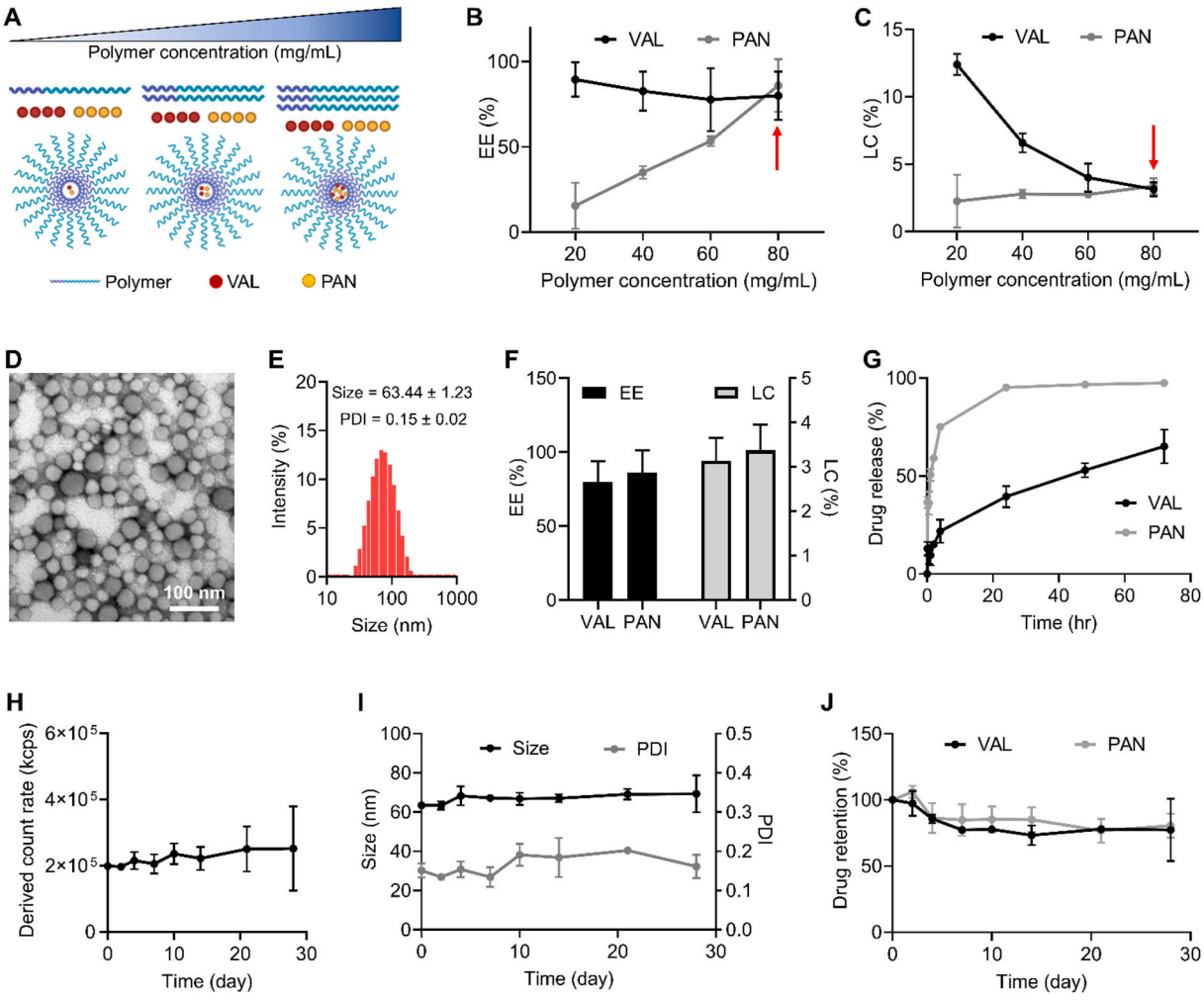

Fig. 3. Generation of mPEG-*b*-p(HPMAm-Bz)-based polymeric micelles co-encapsulating valrubicin and panobinostat. (A) The polymer concentration was systematically increased during micelle formulation to optimize the co-encapsulation of VAL and PAN. (B-C) At 80 mg/mL polymer concentration (red arrows), VAL and PAN showed maximal EE % and were co-loaded at a weight ratio of 1:1. (D) Transmission electron microscopy depicting spherical morphology of the co-loaded micelle formulation. (*E*-F) The micelles exhibited narrow size distribution with EE > 80 % for both drugs. (G) Drug release kinetics at physiologically sink conditions in 4.5 % (*w/v*) albumin-containing PBS media at pH 7.4. VAL was released in a sustained manner, while PAN displayed more rapid release. (H-J) Shelf-stability of the multidrug micelle formulations, illustrating no significant change in the micelle concentration, size, PDI, and drug retention upon 4 weeks of storage at room temperature. Data represent mean ± standard deviation of 3 independent micelle formulations. Statistical analyses in panels H-J were performed using two-way ANOVA, corrected for multiple comparisons. (For interpretation of the references to colour in this figure legend, the reader is referred to the web version of this article.)

co-administered as free drugs over six weeks or until tumor reached a size of 15 mm (Fig. 4A). At the end of the study, tumors were harvested and collected for histological analysis. We hypothesized that the co-loaded micelles would preferentially accumulate in tumors, due to passive endothelial leakiness and permeability processes, as well as to active trans-endothelial transport processes [24,25].

As depicted in Fig. 4B, the tumor growth of subcutaneously inoculated GL261 malignancies was prominently inhibited in mice treated with VAL and PAN double drug-loaded micelles. After the second treatment, the co-loaded micelles demonstrated more than a 3-fold decrease in tumor volume as compared to the free drug combination and to saline treated controls ($p < 0.01$; Fig. 4C). Computed tomography imaging of tumor volumes confirmed the suppression of tumor growth in mice treated with VAL and PAN co-loaded micelles (Fig. 4D). Moreover, the treatment was found to be well tolerated, as evidenced by stable body weights throughout the entire duration of the experiment (Fig. 4E). At the end of the experiment, tumors were harvested, and stained for Ki67 and TUNEL, to assess cell proliferation and apoptosis, respectively. Fluorescence microscopy analysis indicated slightly higher apoptosis induction for tumors treated with multidrug administered in free form or *co*-loaded in polymeric micelles (Fig. 4F-G).

2.4. *Efficacy of double-drug micelles plus sonopermeation in an orthotopic patient-derived diffuse intrinsic pontine glioma mouse model*

We finally evaluated the efficacy of VAL plus PAN co-loaded micelles in mice bearing orthotopic patient-derived DIPG lesions. To this end, we employed the HSJD-DIPG-007 model, which does not allow the extravasation of model drug Evans Blue indicating an intact BBB, a typical characteristic of DIPG lesions in patients [2,26]. The treatment regimen is depicted in Fig. 5A, wherein SonoVue® MB were i.v. administered combined with transcranial focused ultrasound (FUS). Subsequently, VAL and PAN were i.v. administered at a dose of 6 mg/kg either in free form or *co*-encapsulated in polymeric micelles. Treatment was performed once weekly, for a total of two weeks (Fig. 5A).

Representative bioluminescence images (BLI) of luciferase-expressing HSJD-DIPG-007 cells inoculated into the pons of mice showed indications of reduced signals in animals treated with multidrug

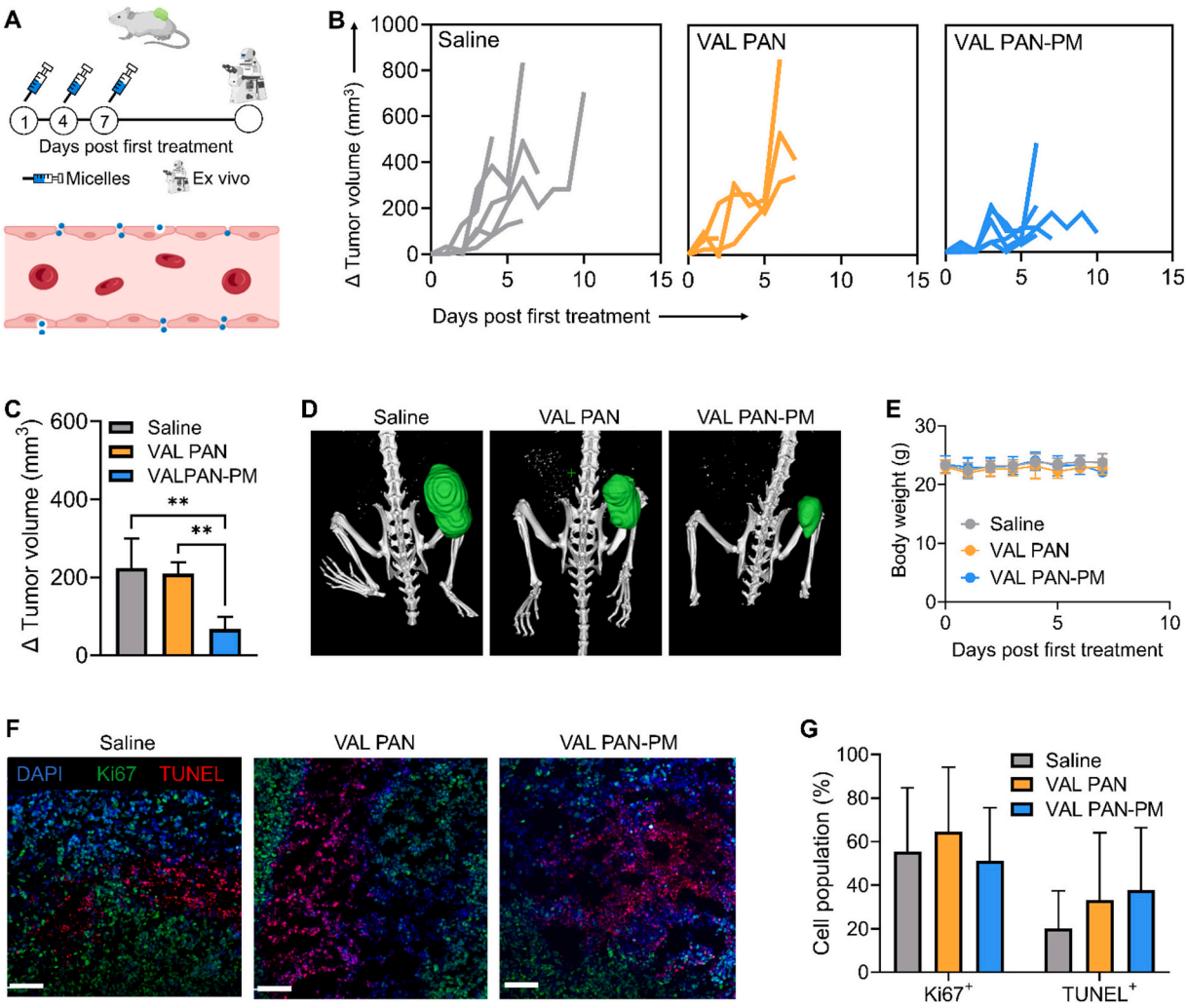

Fig. 4. Valrubicin and panobinostat co-loaded micelles improve therapeutic efficacy in a non-diffuse GL-261 glioma model. (A) GL-261 cells were subcutaneously injected into mice. VAL and PAN were administered intravenously in polymeric micelle (co-loaded; VAL PAN-PM) or in free form (co-administered; VAL PAN), each at a dose of 6 mg/kg, when tumors became palpable. Treatment was performed twice weekly over six weeks or until tumor reached a size of 15 mm. Subsequently, tumors were harvested for ex vivo histological analysis. Micelles were hypothesized to preferentially accumulate in tumors via inter-endothelial gaps or active transport processes, thereby increasing the likelihood of anti-tumor efficacy. (B) Caliper-based tumor volumes of individual mice treated with saline, free VAL PAN and micellar VAL PAN. (C) Mean tumor volume of mice treated with VAL PAN micelles was significantly reduced after the second injection. (D) Representative 3D rendering CT images showing reduced tumor volume in mice treated with VAL PAN micelles. (E) Body weight measurements demonstrating good tolerability of the treatment. (F) Fluorescence microscopy of ex vivo tumor tissues stained for DAPI (nuclei in blue), Ki67 (cell proliferation in green) and TUNEL (apoptosis in red). Scale bar represents 100 μm. (G) Quantitative analysis indicates slightly higher TUNEL signals in case of VAL and PAN co-loaded micelles. Data represent mean ± standard deviation, $N \geq 3$. Statistical analysis for panel C was performed using one-way ANOVA. For panels E and G, two-way ANOVA corrected for multiple comparisons was used. $^{**}p < 0.01$. (For interpretation of the references to colour in this figure legend, the reader is referred to the web version of this article.)

micelles in combination with sonopermeation (Fig. 5B). These findings were most prominent at later time points, i.e., at day 23 and day 35 post treatment (Fig. 5B). Upon plotting absolute BLI signals vs. time curves for individual mice, we observed that combination treatment with VAL and PAN in free form and in micelles together with sonopermeation showed signs of tumor growth inhibition (Fig. 5C). Relative BLI over time curves showed that tumors in the mice treated with double drug-loaded micelles combined with sonopermeation tended to grow slower than tumors treated with the free drugs combined with sonopermeation (Fig. 5C).

When interpreting the results of this orthotopic DIPG tumor growth study, it should be noted that the patient-derived HSJD-DIPG-007 tumor cells that were employed have been previously shown to infiltrate the olfactory bulb [2]. This specific tumor growth feature massively impacts both the smell sensation and the food intake of mice [2]. Consequently, several mice lost body weight and had to be terminated preliminarily during the course of the experiment, compromising the statistics of the treatment read-outs. Furthermore, as this tumor model is known to show slow drug responsiveness, we extrapolated the mean BLI curve until 50 days to predict the treatment efficacy. Mice treated with double drug-loaded micelles and sonopermeation displayed reduced tumor burden by 2–3 folds at day 50 post treatment (Supplementary Fig. S1). Despite being a hard-to-treat and an aggressiveness tumor model, our approach on combining sonopermeation and multidrug polymeric micelles displayed early signs of treatment efficacy.

3. Discussion

Drug delivery to brain tumors is very challenging and typically results in poor treatment efficacy [1,2]. Several strategies have been employed to improve drug targeting and therapeutic outcomes in high-grade brain tumors. For instance, administration of multiple drugs including combinations of indotecan-niraparib and temozolomide-doxorubicin has been used as synergistic drug combinations in brain

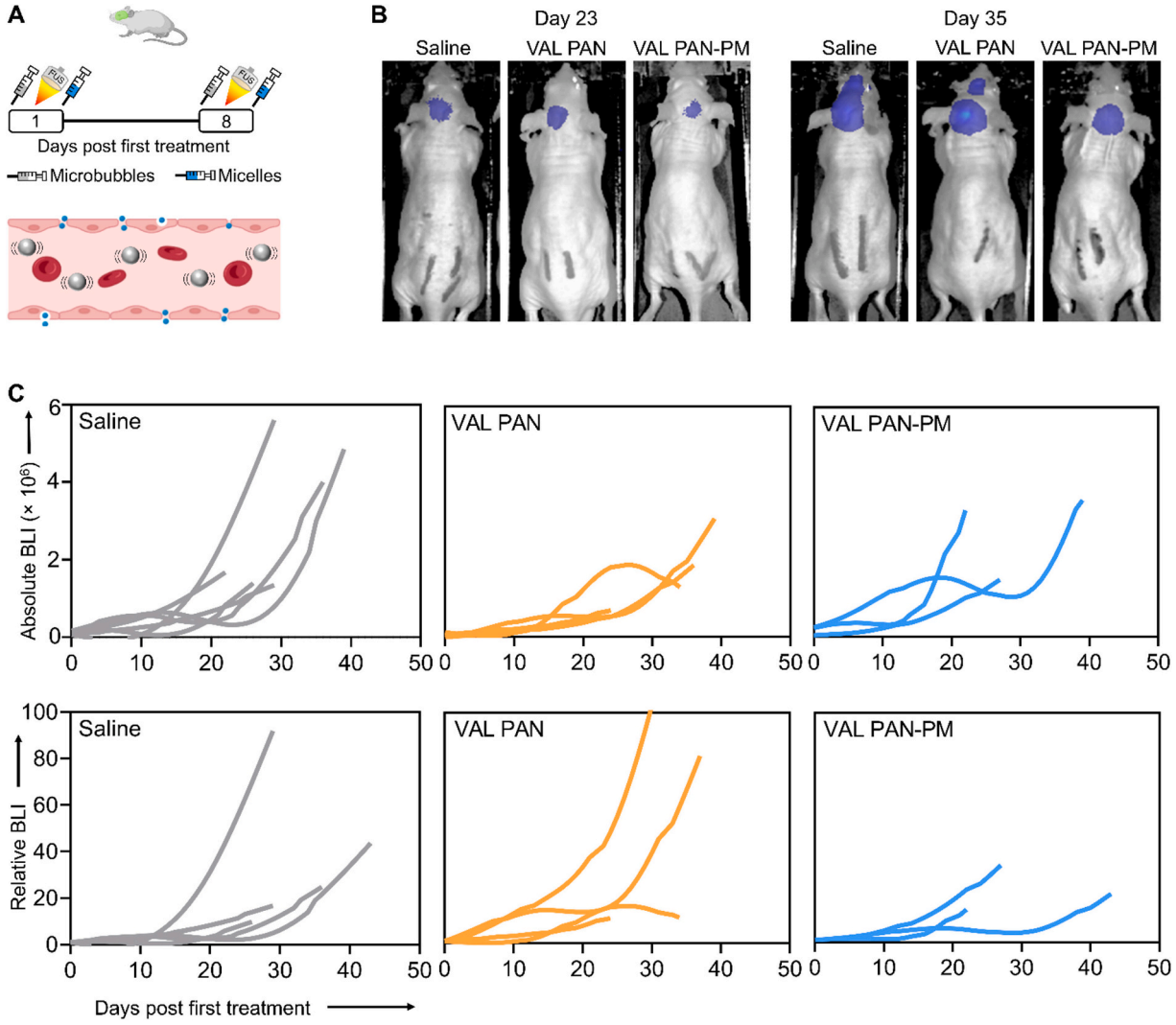

Fig. 5. Multidrug micelles co-loaded with valrubicin and panobinostat combined with sonopermeation show signs of efficacy in orthotopically implanted patient-derived HSJD-DIPG-007 xenograft gliomas in mice. (A) Luciferase-expressing HSJD-DIPG-007 cells were inoculated into the brain stem of mice. At day 14 post tumor implantation, SonoVue® microbubbles were infused, and they were activated by transcranial US to enhance BBB permeation and drug delivery. Immediately afterwards, VAL and PAN were co-administered either in micellar or in free form, at a dose of 6 mg/kg. Treatment was performed once weekly for two weeks, BLI was performed at regular intervals to assess tumor growth and treatment response. (B) Representative BLI images illustrating reduced tumor burden for mice treated with co-loaded micelles and sonopermeation at day 23 and day 35 post treatment. (C) Absolute and relative BLI signals vs. time curves of individual mice treated with saline, free drugs and multidrug micelles in combination with sonopermeation.

tumor treatment [27,28]. Nanomedicines, such as liposomal doxorubicin and albumin-based paclitaxel, have also been explored to enhance anti-tumor efficacy [29]. An increasingly popular strategy is to combine MB and US to permeate the BBB, thereby facilitating the accumulation of drugs and drug delivery systems in the brain. This technology is commonly referred to as sonopermeation, and has been used to deliver olaparib, panobinostat, doxorubicin and Doxil® to high-grade brain tumors [2,16,30–32]. To date, the above-mentioned approaches have mostly been used in glioma models.

We here propose a multipronged nanosonochemotherapy approach, combining (1) a synergistic drug combination, (2) multi-drug nanomedicine and (3) BBB sonopermeation to eventually boost treatment efficacy in hard-to-treat brain cancers. In the context of drug synergism, HDAC inhibitors were combined with anthracyclines as they produced synergistic effects in several glioma cell lines. HDACi are known to cause an increase in histone H3 acetylation, thereby resulting in an open chromatin conformation and transcription. Subsequently, as the DNA becomes more accessible, anthracyclines can intercalate in the DNA more efficiently, thereby inducing synergistic effects [33,34]. Other than brain cancers, HDACi and anthracycline combinations are also known to have synergistic effects also in gastric cancers, breast tumors and lymphoma [33–35]. Next, we developed a nanomedicine formulation incorporating the synergistic drug combination, based on π electron-stabilized polymeric micelles, which can efficiently (co-)load hydrophobic drugs [20–22]. This polymeric micelle platform enabled co-loading of the synergistic drug combination in micelles, and inhibited tumor growth in a subcutaneous glioma model. Previously, the application of sonopermeation has been shown to improve the delivery of small and large molecule therapeutics including ribavirin, dextran and pHPMA polymer – the building block of micelle - in an in vitro BBB model [36,37]. Here, we employed an in vivo orthotopic DIPG model, and found that the application of sonopermeation and multidrug micelles displayed initial signs of efficacy in the pons region of the brain. Regarding the balance between target vs off-target delivery, we have previously shown that FUS application in the pons region in HSJD-DIPG-007 tumor significantly enhances drug accumulation in the pons area, while only modest or no significant drug accumulation was observed in other brain regions [2]. Since our study employed the same

experimental protocol, we strongly believe that FUS application will also likely enhance micelle accumulation in the pons region causing therapeutic efficacy, while no significant accumulation is expected in the off-target brain regions.

Despite these encouraging findings, there are several shortcomings and multiple ways to further improve the performance of multidrug micelles and sonopermeation for brain cancer therapy. First, apart from evaluating the synergistic effects of the free drugs, synergism should also be assessed in vitro for drugs co-encapsulated in micelles. Second, p-glycoprotein (P-gp), a carrier-mediated efflux transporter present in brain tumors, is known to actively pump drugs out of cells and thereby resulting in ineffective drug delivery [38]. To overcome this obstacle, drugs such as P-gp inhibitors can also be co-encapsulated in micelles, to block the efflux of chemotherapy drug molecules and to further enhance drug retention in brain tumors. Third, for achieving enhanced therapeutic efficacy, it will be important to maximize (nano)drug accumulation in brain tumors upon sonopermeation. US settings such as peak-negative pressure, frequency, mechanical index can be optimized to improve the degree of BBB permeability, thereby enhancing drug accumulation [39,40]. Drug properties such as albumin binding capacity or nanoformulation properties such as size, drug loading capacity, active targeting should also be optimized as they can significantly impact free drug vs. nanodrug accumulation [41–43]. Furthermore, antibody-targeted MB can be employed to promote binding to (tumor) blood vessels in the brain, in order to more efficiently permeate the BBB in metastatic lesions and improve (nano)drug accumulation [44]. Fourth, to elucidate the benefit of double drug-loaded micelle, it will be key to systematically study and compare the therapeutic efficacy of dual-drug micelles vs. single drug formulations. Finally, the HSJD-DIPG-007 model employed here grows heterogeneously, complicating efficient ultrasound treatment planning and execution. Moreover, the tumor cells in DIPG models tend to metastasize to the olfactory bulb, causing weight loss and negatively affecting mouse well-being, resulting in preliminary loss of animals from all the groups [2]. Future studies with more and better controllable DIPG models are needed to further explore and confirm the potential of nanosonochemotherapy treatment protocols.

The use of multidrug micelles and sonopermeation may help to improve drug delivery also outside of the brain. For example, in pancreatic cancer, blood vessels are poorly perfused and the stroma is known to be very dense, impeding efficient drug delivery [45]. Also in this situation, sonopermeation may help, as shown previously by Dimcevski and colleagues, who demonstrated that patients with stage IV pancreatic had a median survival time of 18 months upon combining gemcitabine with ultrasound and microbubbles, as compared to only 9 months for gemcitabine alone [46]. In such setups, one could envision nanosonochemotherapy protocols in which micelles or liposomes contain, besides an anticancer drug, also an anti-fibrotic agent, to help degrade the dense collagen matrix in desmoplastic tumor microenvironments, thereby further augmenting drug delivery, penetration and efficacy [47]. Altogether, our efforts exemplify that multidrug nanomedicines combined with sonopermeation hold promise for drug delivery applications in brain cancer and beyond.

4. Conclusion

The combination of anthracyclines and HDACi produced synergistic effects in glioma cell lines. Valrubicin, as an anthracycline, and panobinostat, as a HDACi, were efficiently *co*-loaded in [mPEG-*b*-p(HPMAm-Bz)]-based polymeric micelles. In mice bearing GL-261 glioma model, intravenously administered co-loaded micelles were shown to suppress tumor growth more efficiently than the co-injected free drugs. Finally, in a diffuse glioma model setting, we found that administering co-loaded micelles in combination with microbubbles and focused ultrasound resulted in modest anti-tumor efficacy. These findings highlight the promise of combining multidrug micelles, microbubbles and ultrasound for improving drug delivery to and therapeutic efficacy in brain tumors.

5. Materials and methods

Materials. Panobinostat and vorinostat were purchased from Biochempartners, BCP01816 and Toronto research chemicals, M373425, respectively. Daunorubicin, doxorubicin and epirubicin were obtained from LC Laboratories (US). Idarubicin and pirarubicin were purchsed from AbMole BioScience (US). Valrubicin was bought from United States Pharmacopeia (USA). mPEG-*b*-p(HPMAm-Bz) block copolymer (Mn ~ 22 kDa and D ~ 1.7 based on gel permeation chromatography) was purchased from Chem Connection (now Ardena). SonoVue® was purchased from Bracco. HSJD-DIPG-007 cells were generously provided by Dr. Ángel Montero Carcaboso, Sant Joan de Déu Barcelona Hospital. Milli-Q water was used for all experiments and all other reagents were of appropriate analytical grade.

High-throughput drug screening. Human cell lines used in this study were U-87MG (NCI), GL-261 (ATCC), KNS-42 (japanese Collecotion of Research Bioresources) and SF-8628 Human DIPG H3.3-L27M (Merk). The cells were tested for mycoplasma before use. U-87MG and KNS-42 were routinely cultured in EMEM medium (Sigma) supplemented with 5 % fetal bovine serum (FBS, Sigma Aldrich), 2 mM L-Glutamine (Sigma Aldrich) and 100 U/mL Penicillin–Streptomycin (Thermo Fisher Scientific). SF8628 and GL261 were routinely cultured in DMEM medium (Sigma) supplemented with 10 % fetal bovine serum (FBS, Sigma Aldrich), 2 mM L-Glutamine (Sigma Aldrich) and 100 U/mL Penicillin–Streptomycin (Thermo Fisher Scientific). All cells were maintained at 37 °C with 5 % CO2 and 80 % relative humidity and passaged according to in-house protocols. Cells used in experiments never exceeded passage 25.

Cells were plated with 35 μL complete growth medium in 384-well black tissue culture treated plates (Corning). The seeding numbers for the cells were optimized to ensure that the cells dit not reach full confluency before the endpoint readout. The following seeding desities were used: U-87MG 1800 cells per well, KNS-42 3000 cells per well, GL-261 800 cells per well and SF-8628 300 cells per well. Following seeding, plates were shaken (1,600 rpm, 30 s) to ensure uniform sedimentation of cells. Subsequently, the cells were allowed to adhere for 24 h before drug addition.

For the drug combination screen, all drug compounds were disolved in DMSO to a stock concentration of 1 mg/mL. A Tecan D300 dispenser was used to add the drug compounds in combinations and as single drugs to assay plates with the various cells. All drug compounds were tested at 4 concentrations (1, 10, 100, 1000 ng/mL) alone and in pairwise combinations with the other drug compounds. Assay wells without the addition of drug compounds were included as referance. DMSO was added to the assay wells to normalize the DMSO concentration to 0.5 %. Three technical replicates on separate plates were included for all conditions. Cells were incubated at 37 °C with 5 % CO2 and 80 % relative humidity. Cell viability was assessed by reading luminescence after 10 min incubation with the CellTiter-Glo 2.0 reagent (20 μL/well, mixed 1:1 with PBS prior to addition) in a Beckman Coulter liquid handling robotic system with an integrated Molecular Devices SpectraMax i3x microplate reader. Drug synergy was evaluated by calculating Bliss excess synergy index based on the average viability of the assay wells relative to the viability in untreated control wells according to the formulae below [48]. Negative and positive values indicate synergistic and antagonistic effects, respectively.

$$\text{Bliss excess} = \text{Viability (Drug A + Drug B)} - \text{Viability (Drug B)} \times \text{Viability (Drug A)} \quad (1)$$

Multidrug micelle preparation. Valrubicin and panobinostat *co*-loaded polymeric micelles were prepared via a nanoprecipitation method [20]. To optimize the micelle formulation, different

concetrations of the mPEG-*b*-p(HPMAm-Bz) block copolymers (20, 40, 60 and 80 mg) were mixed with 3 mg of valrubicin and 3 mg of panobinostat and dissolved in 1 mL of THF:methanol (1:1) organic phase. The solutions were added dropwise to 1 mL of Milli-Q water under vigorous stirring at 1000 rpm for 2 min. Subsequently, the samples were kept at RT for 48 h to allow evaporation of THF and methanol. The micellar suspension was centrifuged at 5000 *g* for 10 min to remove any precipitate, and the supernatant was collected. Later, the volume of the micellar formulations was adjusted to 1 mL with Milli-Q water, and the suspensions were filtered through a 0.45 μm polyethersulfone (PES) filter. Finally, the micelle formulations were stored at 4^0C until further use.

Dynamic light scattering. The hydrodynamic diameter (*Z*-average, size) and polydispersity index (PDI) of valrubicin and panobinostat co-loaded micelles were evaluated using a Zetasizer Nanoseries ZS90 (Malvern instruments Ltd., UK). DLS samples were prepared by diluting 50 μL of the micelle formulations in 950 μL of Milli-Q water in disposable polystyrene cuvettes. All samples were measured 3 times with 10 runs per measurement at 25 °C. Finally, size, PDI, and size distribution histograms of the co-loaded micelles were derived based on the autocorrelation function.

Transmission electron microscopy. The co-loaded micelles were diluted 1000-fold in Milli-Q water. The samples were adsorbed on glow discharged formvar-carbon-coated nickel grids (Maxtaform, 200 mesh, Plano, Wetzlar, Germany) for 10 min. TEM images were examined using a Hitachi HT7800 TEM (Hitachi, Tokyo, Japan), operating at an acceleration voltage of 100 kV.

High performance liquid chromatography. To evaluate the loading efficiency of panobinostat in the micelles, 50 μL of VAL PAN micelles were diluted in 450 μL of ACN and methanol (1:1) to dissolve both the polymers and the drugs. Subsequently, the solution was filtered through 0.2 μm PTFE filters, and the amount of panobinostat was quantified using reversed-phase HPLC (1260 II Infinity LC system, Agilent technologies, USA). For the mobile phase, a gradient elution method was used with a ACN/water mixture ranging from 39/61 (v/v) to 65/35 (v/v), and contained 0.1 % trifluoroacetic acid in each solvent. The injection volume was 25 μL and the samples were measured at a flow rate of 1 mL/min using a C18 column (4.6 × 150 mm, 5 μm) as a stationary phase. Calibration curve of panobinostat at 227 nm was generated and was utilized to quantify the panobinostat encapsulation in the micelles using the integrated area under the peak.

Panobinostat EE % and LC % was calculated as follows:

$$EE = \frac{\text{weight of panobinostat loaded into micelles}}{\text{feed weight of panobinostat}} \times 100\% \quad (2)$$

$$LC = \frac{\text{weight of panobinostat loaded into micelles}}{\text{weight of loaded panobinostat and polymer}} \times 100\% \quad (3)$$

Fluorescence plate reader. To quantify valrubicin content, 10 μL of co-loaded micelles were diluted in 90 μL of DMSO. This step destroyed the micelles and dissolved the polymer and drug. The amount of valrubicin incorporated into the micelles was then quantified using a microplate reader TECAN Infinite M200 Pro (Tecan Group Ltd., Germany). The fluorescence excitation wavelength was set at 498 nm and the emission wavelength was 596 nm. Finally, EE and LC were determined as follows:

$$EE = \frac{\text{weight of valrubicin loaded into micelles}}{\text{feed weight of valrubicin}} \times 100\% \quad (4)$$

$$LC = \frac{\text{weight of valrubicin loaded into micelles}}{\text{weight of loaded valrubicin and polymer}} \times 100\% \quad (5)$$

Drug release. The release profiles of valrubicin and panobinostat from the micelles were evaluated under sink conditions. A solution of 4.5 % bovine serum albumin (BSA)- in PBS at pH 7.4 was used as the medium. The co-loaded micelles were transferred into a Float-A-Lyzer dialysis device (300 kDa MWCO), and the dialysis device was submerged in the medium at 37 °C under continuous shaking. 50 μL of the sample was withdrawn from the dialysis device at different time points. To compensate the loss in volumes from the dialysis devices, 50 μL of fresh medium was added. The withdrawn samples were diluted 10-fold in a mixture of ACN and methanol (1:1), and centrifuged at 5000 *g* for 10 min to remove the precipitated BSA. Subsequently, the amount of drug in the supernatant was determined via HPLC (Panobinostat) or fluorescence plate reader (valrubicin), as explained above. Finally, the release % of panobinostat and valrubicin were evaluated by subtracting the % content in the supernatant from 100 %.

Stability of multidrug micelles. Valrubicin and panobinostat co-loaded micelles in Milli-Q water were stored at room temperature for stability evaluation. The derived count rate, size and PDI were measured by DLS. The retention of valrubicin and panobinostat inside the micelles were studied over a period of 4 weeks using fluorescence plate reader or HPLC, respectively.

Cell culture. GL-261 cells were maintained in Dulbecco's Modified Eagle's Medium—4.5 g/L glucose (ThermoFisher) supplemented with 10 % fetal bovine serum (PAN-Biotech) and 1 % penicillin-streptomycin (10,000 U/mL). Cells were maintained at 37 °C in a humidified incubator with 5 % CO_2, and passaged every 3–4 days. HSJD-DIPG-007 cells were obtained from the University of Barcelona and were grown as suspension cultures in 1:1 Neurobasal-A and Advanced DMEM/F-12 medium containing 10 mM HEPES buffer, 1 × MEM non-essential amino acids, 1 % GlutaMAX, 1 mM sodium oyruvate, 1 × B-27 minus vitamin-A, 10 ng/mL PDGF-AA, 10 ng/mL PDGF-BB (ThermoFisher), 20 ng/mL bFGF, 20 ng/mL EGF (Princess Maxima Center pharmacy), 2 μg/mL heparin (StemCell Technologies) and 1 mg/mL primocin (InvivoGen). Furthermore, these cells were transduced to express firefly luciferase using a previously described protocol, to enable in vivo bioluminescence imaging of tumor growth [49].

Animal experiments. All animal procedures on the GL-261 mouse model were approved by the German State Office for Nature, Environment and Consumer Protection (LANUV) North Rhine-Westphalia. All experiments were performed in adherence to institutional guidelines, EU Directive 2010/63/EU, and the German federal law on the protection of animals. All animal procedures on the DIPG-HSDJ-007 model were performed in accordance with guidelines of the Dutch Ethical Committee and the Animal Welfare Body of Utrecht University (AVD3990020209445, approval date: 11/02/2020). In these studies, injections were administered i.v. into the lateral tail vein unless stated otherwise.

In vivo therapy study in subcutaneous GL-261 model. 100,000 GL-261 cancer cells were subcutaneously injected into the flank of BALB/cAnN-*Fox1*$_{nu/nu}$/Rj mice (female mice, 4–8 weeks old, Janvier Labs). Mice were housed 20–24 °C, with 12 h light/dark cycle, a humidity of 45–65 % and under specific pathogen-free conditions, according to the guidelines of the "Federation for Laboratory Science Associations" (FELASA). Food and water were offered ad libitum and mice were housed in groups of up to 5. They were assigned individual earmarks enabling identification and randomly distributed in the treatment groups. The daily monitroing of each animal as well as performing the experiments were done by two experienced unblinded researchers. Treatment was started when tumors became palpable. Mice were randomly divided in three groups, $n = 5$: (i) saline, (ii) 6 mg/kg valrubicin and panobinostat in free form, (iii) 6 mg/kg valrubicin and panobinostat in micellar form. Treatment was continued for six weeks or until the tumor reached 15 mm in one dimension. Intravenous injections and CT imaging were performed on anesthetized mice. Inhalation anesthesia was induced in a chamber (Drägerwerk AG, Lübeck, Germany) using 5 Vol% isoflurane (Forene, Abbott, Wiesbaden, Germany) in oxygen, and maintained at 2–2.5 Vol%. The tumor size was evaluated daily via caliper measurements (width, w and length, l). To validate the tumor sizes, micro-computed tomography of the whole body was performed at the beginning and end of the experiment using the U-CT

device (MILabs B.V. a Rigaku Company, Utrecht, The Netherlands). In a full-rotation in step-and-shoot mode, 480 projections (1944 × 1536 pixels) were acquired with an X-ray tube voltage of 55 kV, power 0.17 mA, exposure time of 75 ms, and low-dose (≈0.1 Gy/whole body scan). To cover the entire animal, two subscans were acquired. Imaging data was processed and reconstructed using the Imalytics Preclinical software (Gremse-IT GmbH, Germany) for segmentation and analysis of the tumor size [50]. Mice were killed during isoflurane anesthesia via cervical dislocation. The tumor volume was calculated as follows:

$$V = \frac{l}{2} \times w^2 \quad (5)$$

In vivo therapy study in orthotopic HSJD-DIPG-007 model. The HSJD-DIPG-007 model was obtained according to 't Hart et al. [26]. Briefly, 6–8-week-old male Hsd:Athymic Nude-Foxn1^{nu} mice (Envigo, Horst, The Netherlands) were anesthetized by isoflurane and fixed in a stereotaxic platform. The skin on the scull was opened and a small hole was drilled at 0.8 mm posterior and 1.0 mm lateral to the lambda. Subsequently, a needle (5 μL Hamilton syringe fitted with a 26-gauge needle) was inserted 4.5 mm into the brain to reach the pontine area of the mouse. 0.5×10^6 cells in saline were injected at a rate of 2 μL/min. The needle stayed in this position for 7 mins before the needle was slowly removed from the brain. Before and after surgery, the animals were provided carprofen in the drinking water. Before the hole was drilled, lidocaine was placed on the skull.

Subsequently, 14 days after tumor injection, animals were treated with sonopermeation, after which VAL and PAN in free form or VAN and PAL co-loaded micelles were injected. The sonopermeation is described in detail by 't Hart and Haumann et al. [51]. Briefly, animals were provided buprenorphine s.c. before sonopermeation. Subsequently, animals were anesthesized by isoflurane and mounted on a stereotaxic platform. Animals were i.p. administrated with 150 mg/kg D-luciferin. A BLI image was acquired and was loaded into the software and the tumor was localized. Mice were then placed onto the stereotactic platform and a hydrophone (Precision Acoustics, United Kingdom) was positioned behind the left ear of the animal to monitor scattered cavitation signal. 60 μL of SonoVue® MB were i.v. administered, and FUS was applied at 1 MHz, with 1.6 Hz pulse repetition frequency and 400 kPa pressure, in a hexagonal pattern of 10 millisecond tone bursts. Later, VAL and PAN in free form or VAL and PAN co-loaded micelles were injected. After treatment, the tumor was monitored thrice by BLI imaging. Briefly, the mice were anesthetized by isoflurane and 150 mg/kg D-luciferin was i.p. injected in the mouse. Subsequently, an image was performed by the BLI and peak intensity was used to analyse the data. Absolute BLI was plotted to demonstrate the heterogeneity in the starting tumor volumes and growth curves. Furthermore, relative BLI, i.e. the ratio of BLI at day X to day 0, was also plotted to ensure that all mice had same starting relative BLI values, thereby enabling head-to-head comparisons in tumor growth kinetics between the groups.

Histology. After sacrificing the mice, tumors were excised and embedded in specimen matrix for cryosectioning (Tissue-Tek OCT, Sakura, USA). Frozen tumor tissue was cut in 10 μm slices using a cryotome (Cryostat CM3050 S, Leica Biosystems, Nussloch, Germany). The tumor sections were fixed with 4 % PFA for 15 min, followed by three times washing in PBS for 10 min. The cells were permeabilized using each 0.1 % of Triton-X-100 and sodium citrate in aqua dest for 2 min, followed by three times washing in PBS for 10 min. For (immuno) fluorescence stainings, apoptotic (TUNEL) and proliferating (Ki-67) cells were marked using a TUNEL staining kit (Roche) and an anti-Ki-67 antibody (#ab15580, Abcam). TUNEL and antibodies incubation was always performed in a humidified chamber in the dark, followed by a DAPI staining (Merck) and three times PBS washing for 10 min. Finally, slides were mounted with Mowiol (Carl Roth) and glass-covered. A total of 8 images per animal were stained, and 10× objective was used to image large areas (900 × 676 μm) with an average of 3,000 cells per image. Images were acquired using an AxioImager M2 microscopy system with an AxioCamMRm Rev.3 camera (Carl Zeiss Microscopy Deutschland GmbH). Representative images were used to count apoptotic and proliferating cells using QuPath [52].

Statistical analysis. Data are represented as mean ± standard deviation. All results were analyzed using GraphPad Prism 9.1.1. Statistical analysis was performed using one-way ANOVA, or two-way ANOVA corrected for multiple comparisons, as indicated in the figure legends. Significance was determined at the following cutoff points: * $p < 0.05$, ** $p < 0.01$, *** $p < 0.001$ and **** $p < 0.0001$.

CRediT authorship contribution statement

Anshuman Dasgupta: Writing – original draft, Visualization, Methodology, Investigation, Formal analysis, Conceptualization. **Jan-Niklas May:** Writing – review & editing, Visualization, Methodology, Investigation, Formal analysis, Conceptualization. **Geir Klinkenberg:** Writing – review & editing, Methodology, Investigation. **Helena C. Besse:** Writing – review & editing, Methodology, Investigation. **Eva Miriam Buhl:** Resources, Methodology, Investigation. **Diana Moeckel:** Methodology, Investigation. **Rahaf Mihyar:** Writing – review & editing, Investigation. **Quim Peña:** Writing – review & editing, Investigation. **Armin Azadkhah Shalmani:** Writing – review & editing, Investigation. **Christopher Hark:** Methodology, Investigation. **Anne Rix:** Writing – review & editing, Methodology, Investigation. **Susanne Koletnik:** Methodology, Investigation. **Josbert Metselaar:** Writing – review & editing, Investigation. **Yang Shi:** Methodology. **Wim E. Hennink:** Writing – review & editing, Investigation. **Gert Storm:** Writing – review & editing, Investigation. **Dannis van Vuurden:** Writing – review & editing, Funding acquisition. **Chrit Moonen:** Writing – review & editing, Investigation, Funding acquisition. **Mario Ries:** Writing – review & editing, Visualization, Supervision, Project administration. **Ruth Schmid:** Writing – review & editing, Investigation, Funding acquisition. **Fabian Kiessling:** Writing – review & editing, Visualization, Funding acquisition. **Twan Lammers:** Writing – review & editing, Visualization, Supervision, Project administration, Funding acquisition, Conceptualization.

Declaration of competing interest

The authors have no relevant conflicts of interest to declare.

Acknowledgements

The authors gratefully acknowledge support by the European Commission (EuroNanoMed-III: NSC4DIPG), the European Research Council (ERC-CoG 864121: Meta-Targeting), the German Federal Ministry of Research and Education (BMBF: Gezielter Wirkstofftransport, PP-TNBC, 16GW0319K), and the German Research Foundation (DFG: GRK/RTG2375 (grant #331065168), SFB1066, FOR5011, and LA2937/4-1). BioRender software (https://biorender.com) was employed for creating schematics.

Appendix A. Supplementary data

Supplementary data to this article can be found online at https://doi.org/10.1016/j.jconrel.2025.02.018.

Data availability

Data will be made available on request.

References

[1] W.M. Pardridge, Drug transport across the blood–brain barrier, J. Cereb. Blood Flow Metab. 32 (11) (2012) 1959–1972.
[2] J. Bianco, M.A.C. Bruin, M. Derieppe, H.C. Besse, K. Berkhout, L.C.J. Kie, Y. Su, E. W. Hoving, A.D.R. Huitema, M.G. Ries, D.G. van Vuurden, Radiosensitisation by

olaparib through focused ultrasound delivery in a diffuse midline glioma model, J. Control. Release 357 (2023) 287–298.
[3] S.Y. Qin, Y.J. Cheng, Q. Lei, A.Q. Zhang, X.Z. Zhang, Combinational strategy for high-performance cancer chemotherapy, Biomaterials 171 (2018) 178–197.
[4] T. Ojha, V. Pathak, Y. Shi, W.E. Hennink, C.T. Moonen, G. Storm, F. Kiessling, T. Lammers, Pharmacological and physical vessel modulation strategies to improve EPR-mediated drug targeting to tumors, Adv. Drug Deliv. Rev. 119 (2017) 44–60.
[5] A. Dasgupta, M. Liu, T. Ojha, G. Storm, F. Kiessling, T. Lammers, Ultrasound-mediated drug delivery to the brain: principles, progress and prospects, Drug Discov. Today Technol. 20 (2016) 41–48.
[6] N.J. Abbott, A.A. Patabendige, D.E. Dolman, S.R. Yusof, D.J. Begley, Structure and function of the blood–brain barrier, Neurobiol. Dis. 37 (1) (2010) 13–25.
[7] G.L. Lin, K.M. Wilson, M. Ceribelli, B.Z. Stanton, P.J. Woo, S. Kreimer, E.Y. Qin, X. Zhang, J. Lennon, S. Nagaraja, P.J. Morris, Therapeutic strategies for diffuse midline glioma from high-throughput combination drug screening, Sci. Transl. Med. 11 (519) (2019) eaaw0064.
[8] L.A. Parsels, D.R. Wahl, C. Koschmann, M.A. Morgan, Q. Zhang, Developing H3K27M mutant selective radiosensitization strategies in diffuse intrinsic pontine glioma, Neoplasia 37 (2023) 100881.
[9] D. Peer, J.M. Karp, S. Hong, O.C. Farokhzad, R. Margalit, R. Langer, Nanocarriers as an emerging platform for cancer therapy, Nano-Enabled Med. Appl. (2020) 61–91.
[10] R. van der Meel, E. Sulheim, Y. Shi, F. Kiessling, W.J. Mulder, T. Lammers, Smart cancer nanomedicine, Nat. Nanotechnol. 14 (11) (2019) 1007–1017.
[11] M. Biscaia-Caleiras, N.A. Fonseca, A.S. Lourenço, J.N. Moreira, S. Simões, Rational formulation and industrial manufacturing of lipid-based complex injectables: landmarks and trends, J. Control. Release 373 (2024) 617–639.
[12] T. Sun, Y. Zhang, C. Power, P.M. Alexander, J.T. Sutton, M. Aryal, N. Vykhodtseva, E.L. Miller, N.J. McDannold, Closed-loop control of targeted ultrasound drug delivery across the blood–brain/tumor barriers in a rat glioma model, Proc. Natl. Acad. Sci. 114 (48) (2017) E10281–E10290.
[13] A. Dasgupta, T. Sun, R. Palomba, E. Rama, Y. Zhang, C. Power, D. Moeckel, M. Liu, A. Sarode, M. Weiler, A. Motta, Nonspherical ultrasound microbubbles, Proc. Natl. Acad. Sci. 120 (13) (2023) e2218847120.
[14] A. Dasgupta, T. Sun, E. Rama, A. Motta, Y. Zhang, C. Power, D. Moeckel, S. M. Fletcher, M. Moosavifar, R. Barmin, C. Porte, Transferrin receptor-targeted nonspherical microbubbles for blood–brain barrier sonopermeation, Adv. Mater. 35 (52) (2023) 2308150.
[15] T. Mainprize, N. Lipsman, Y. Huang, Y. Meng, A. Bethune, S. Ironside, C. Heyn, R. Alkins, M. Trudeau, A. Sahgal, J. Perry, Blood-brain barrier opening in primary brain tumors with non-invasive MR-guided focused ultrasound: a clinical safety and feasibility study, Sci. Rep. 9 (1) (2019) 321.
[16] A. Carpentier, R. Stupp, A.M. Sonabend, H. Dufour, O. Chinot, B. Mathon, F. Ducray, J. Guyotat, N. Baize, P. Menei, J. de Groot, Repeated blood–brain barrier opening with a nine-emitter implantable ultrasound device in combination with carboplatin in recurrent glioblastoma: a phase I/II clinical trial, Nat. Commun. 15 (1) (2024) 1650.
[17] L.M. Arms, R.J. Duchatel, E.R. Jackson, P.G. Sobrinho, M.D. Dun, S. Hua, Current status and advances to improving drug delivery in diffuse intrinsic pontine glioma, J. Control. Release 370 (2024) 835–865.
[18] E.G. Graham-Gurysh, A.B. Murthy, K.M. Moore, S.D. Hingtgen, E.M. Bachelder, K. M. Ainslie, Synergistic drug combinations for a precision medicine approach to interstitial glioblastoma therapy, J. Control. Release 323 (2020) 282–292.
[19] C.S. Grasso, Y. Tang, N. Truffaux, N.E. Berlow, L. Liu, M.A. Debily, M.J. Quist, L. E. Davis, E.C. Huang, P.J. Woo, A. Ponnuswami, Functionally defined therapeutic targets in diffuse intrinsic pontine glioma, Nat. Med. 21 (6) (2015) 555–559.
[20] Y. Shi, R. Van Der Meel, B. Theek, E. Oude Blenke, E.H. Pieters, M.H. Fens, J. Ehling, R.M. Schiffelers, G. Storm, C.F. Van Nostrum, T. Lammers, Complete regression of xenograft tumors upon targeted delivery of paclitaxel via Π–Π stacking stabilized polymeric micelles, ACS Nano 9 (4) (2015) 3740–3752.
[21] R. Mihyar, A.A. Shalmani, V. Wildt, M. Sheybanifard, A. Wang, J.N. May, S. Shahzad, E.M. Buhl, S. Rütten, D. Behrens, W. Walther, Microfluidic formulation, cryoprotection and long-term stability of paclitaxel-loaded π electron-stabilized polymeric micelles, J. Control. Release 375 (2024) 614–626.
[22] A.A. Shalmani, A. Wang, Z. Ahmed, M. Sheybanifard, R. Mihyar, E.M. Buhl, M. Pohl, W.E. Hennink, F. Kiessling, J.M. Metselaar, Y. Shi, Tunable polymeric micelles for taxane and corticosteroid co-delivery, Drug Deliv. Transl. Res. 14 (10) (2024) 2642–2654.
[23] L.H. Snyder, Estimating GL-261 Cell Growth: A Murine Model for Glioblastoma Multiforme, 2014.
[24] L.N. Nguyen, W. Ngo, Z.P. Lin, S. Sindhwani, P. MacMillan, S.M. Mladjenovic, W. C. Chan, The mechanisms of nanoparticle delivery to solid tumours, Nat. Rev. Bioeng. 2 (3) (2024) 201–213.
[25] A. Dasgupta, A.M. Sofias, F. Kiessling, T. Lammers, Nanoparticle delivery to tumours: from EPR and ATR mechanisms to clinical impact, Nat. Rev. Bioeng. (2024) 1–3.
[26] E. Hart, J. Bianco, H.C. Besse, L.A. Chin Joe Kie, L. Cornet, K.L. Eikelenboom, T. J. van den Broek, M. Derieppe, Y. Su, E.W. Hoving, M.G. Ries, Towards standardisation of a diffuse midline glioma patient-derived xenograft mouse model based on suspension matrices for preclinical research, Biomedicines 11 (2) (2023) 527.
[27] O. Kim, M. Butler, Z. Sergi, R.W. Robey, M. Zhang, R. Chari, Y. Pang, G. Yu, W. Zhang, H. Song, D. Davis, Combined inhibition of topoisomerase I and poly (ADP-ribose) polymerase: A synergistic therapeutic strategy for glioblastoma with phosphatase and tensin homolog deficiency, Neuro-Oncol. Adv. 5 (1) (2023) vdad102.
[28] L. Dhungel, M.E. Rowsey, C. Harris, D. Raucher, Synergistic effects of Temozolomide and doxorubicin in the treatment of glioblastoma Multiforme: enhancing efficacy through combination therapy, Molecules 29 (4) (2024) 840.
[29] T. Lammers, F. Kiessling, M. Ashford, W. Hennink, D. Crommelin, G. Storm, Cancer nanomedicine: is targeting our target? Nat. Rev. Mater. 1 (9) (2016) 1–2.
[30] J. Park, M. Aryal, N. Vykhodtseva, Y.Z. Zhang, N. McDannold, Evaluation of permeability, doxorubicin delivery, and drug retention in a rat brain tumor model after ultrasound-induced blood-tumor barrier disruption, J. Control. Release 250 (2017) 77–85.
[31] H.J. Wei, A. Pouliopoulos, N. Yoh, M. Tazhibi, N. McQuillan, X. Zhang, L. Szalontay, R. Gartrell, P. Jovana, Z. Zhang, N. Feldstein, Focused ultrasound-mediated blood-brain barrier opening enhances panobinostat efficacy in a murine diffuse intrinsic pontine glioma model, Int. J. Radiat. Oncol. Biol. Phys. 111 (3) (2021) e177.
[32] https://www.sickkids.ca/en/news/archive/2023/world-first-sunnybrook-sickkids-clinical-trial-chemotherapy-pediatric-brain-tumours-mri-guided-focused-ultrasound/.
[33] B. Sanchez-Gonzalez, H. Yang, C. Bueso-Ramos, K. Hoshino, A. Quintas-Cardama, V.M. Richon, G. Garcia-Manero, Antileukemia activity of the combination of an anthracycline with a histone deacetylase inhibitor, Blood 108 (4) (2006) 1174–1182.
[34] L. Hontecillas-Prieto, R. Flores-Campos, A. Silver, E. De Álava, N. Hajji, D.J. García-Domínguez, Synergistic enhancement of cancer therapy using HDAC inhibitors: opportunity for clinical trials, Front. Genet. 11 (2020) 578011.
[35] G. Lu, S. Jin, S. Lin, Y. Gong, L. Zhang, J. Yang, W. Mou, J. Du, Update on histone deacetylase inhibitors in peripheral T-cell lymphoma (PTCL), Clin. Epigenetics 15 (1) (2023) 124.
[36] C. Hark, J. Chen, J. Blöck, E.M. Buhl, H. Radermacher, R. Pola, M. Pechar, T. Etrych, Q. Peña, A. Rix, N.I. Drude, RGD-coated polymeric microbubbles promote ultrasound-mediated drug delivery in an inflamed endothelium-pericyte co-culture model of the blood-brain barrier, Drug Deliv. Transl. Res. (2024) 1–13.
[37] L. Chen, R. Sutharsan, J.L. Lee, E. Cruz, B. Asnicar, T. Palliyaguru, J. M. Wasielewska, A. Gaudin, J. Song, G. Leinenga, J. Götz, Claudin-5 binder enhances focused ultrasound-mediated opening in an in vitro blood-brain barrier model, Theranostics 12 (5) (2022) 1952.
[38] J.H. Lin, M. Yamazaki, Role of P-glycoprotein in pharmacokinetics: clinical implications, Clin. Pharmacokinet. 42 (2003) 59–98.
[39] N. McDannold, N. Vykhodtseva, K. Hynynen, Blood-brain barrier disruption induced by focused ultrasound and circulating preformed microbubbles appears to be characterized by the mechanical index, Ultrasound Med. Biol. 34 (5) (2008) 834–840.
[40] M. Aryal, C.D. Arvanitis, P.M. Alexander, N. McDannold, Ultrasound-mediated blood–brain barrier disruption for targeted drug delivery in the central nervous system, Adv. Drug Deliv. Rev. 72 (2014) 94–109.
[41] J.N. May, S.K. Golombek, M. Baues, A. Dasgupta, N. Drude, A. Rix, D. Rommel, S. Von Stillfried, L. Appold, R. Pola, M. Pechar, Multimodal and multiscale optical imaging of nanomedicine delivery across the blood-brain barrier upon sonopermeation, Theranostics 10 (4) (2020) 1948.
[42] B. Marty, B. Larrat, M. Van Landeghem, C. Robic, P. Robert, M. Port, D. Le Bihan, M. Pernot, M. Tanter, F. Lethimonnier, S. Mériaux, Dynamic study of blood–brain barrier closure after its disruption using ultrasound: a quantitative analysis, J. Cereb. Blood Flow Metab. 32 (10) (2012) 1948–1958.
[43] M. Olsman, V. Sereti, M. Mühlenpfordt, K.B. Johnsen, T.L. Andresen, A. J. Urquhart, C. de Lange Davies, Focused ultrasound and microbubble treatment increases delivery of transferrin receptor-targeting liposomes to the brain, Ultrasound Med. Biol. 47 (5) (2021) 1343–1355.
[44] V.A. Johanssen, J.L. Ruan, O. Vince, A. Thomas, S. Peeters, M.S. Soto, J. Buck, M. Gray, E. Stride, N.R. Sibson, Targeted opening of the blood-brain barrier using VCAM-1 functionalised microbubbles and "whole brain" ultrasound, Theranostics 14 (10) (2024) 4076.
[45] V.P. Chauhan, T. Stylianopoulos, Y. Boucher, R.K. Jain, Delivery of molecular and nanoscale medicine to tumors: transport barriers and strategies, Annu. Rev. Chem. Biomol. Eng. 2 (1) (2011) 281–298.
[46] G. Dimcevski, S. Kotopoulis, T. Bjånes, D. Hoem, J. Schjøtt, B.T. Gjertsen, M. Biermann, A. Molven, H. Sorbye, E. McCormack, M. Postema, A human clinical trial using ultrasound and microbubbles to enhance gemcitabine treatment of inoperable pancreatic cancer, J. Control. Release 243 (2016) 172–181.
[47] B. Diop-Frimpong, V.P. Chauhan, S. Krane, Y. Boucher, R.K. Jain, Losartan inhibits collagen I synthesis and improves the distribution and efficacy of nanotherapeutics in tumors, Proc. Natl. Acad. Sci. 108 (7) (2011) 2909–2914.
[48] C.I. Bliss, The toxicity of poisons applied jointly 1, Ann. Appl. Biol. 26 (3) (1939) 585–615.

[49] M.W. Kholosy, M. Derieppe, F. van den Ham, K. Ober, Y. Su, L. Custers, L. Schild, M.J.L. van Zogchel, M.L. Wellens, R.H. Ariese, C.L. Szanto, Neuroblastoma and DIPG organoid coculture system for personalized assessment of novel anticancer immunotherapies, J. Pers. Med. 11 (9) (2021) 869.
[50] F. Gremse, M. Stärk, J. Ehling, J.R. Menzel, T. Lammers, F. Kiessling, Imalytics preclinical: interactive analysis of biomedical volume data, Theranostics 6 (3) (2016) 328.
[51] R. Haumann, M.P. Derieppe, H.C. Besse, G.J. Kaspers, E. Hoving, D.G. van Vuurden, E. Hulleman, M. Ries, A high-throughput image-guided stereotactic neuronavigation and focused ultrasound system for blood-brain barrier opening in rodents, J. Vis. Exp. 161 (2020) e61269.
[52] P. Bankhead, M.B. Loughrey, J.A. Fernández, Y. Dombrowski, D.G. McArt, P. D. Dunne, S. McQuaid, R.T. Gray, L.J. Murray, H.G. Coleman, J.A. James, QuPath: open source software for digital pathology image analysis, Sci. Rep. 7 (1) (2017) 1–7.